Title

Flagged uniform particle splitting for variance reduction in proton and carbon ion track-structure simulations

Permalink
https://escholarship.org/uc/item/9vc34905

Journal
Physics in Medicine and Biology, 62(15)

ISSN
0031-9155

Authors
Ramos-Méndez, José
Schuemann, Jan
Incerti, Sebastien
et al.

Publication Date
2017-08-07

DOI
10.1088/1361-6560/aa7831

Peer reviewed

Published in final edited form as:
Phys Med Biol. ; 62(15): 5908–5925. doi:10.1088/1361-6560/aa7831.

Flagged uniform particle splitting for variance reduction in proton and carbon ion track-structure simulations

José Ramos-Méndez[1], **Jan Schuemann**[2], **Sebastien Incerti**[4,5], **Harald Paganetti**[2], **Reinhard Schulte**[1], and **Bruce Faddegon**[1]

[1]Department of Radiation Oncology, University of California San Francisco, CA, USA

[2]Department of Radiation Oncology, Massachusetts General Hospital and Harvard Medical School, MA, USA

[4]CNRS, IN2P3, CENBG, UMR 5797, F-33170 Gradignan, France

[5]Université de Bordeaux, CENBG, UMR 5797, F-33170 Gradignan, France

Abstract

Flagged uniform particle splitting was implemented with two methods to improve the computational efficiency of Monte Carlo track structure simulations with TOPAS-nBio by enhancing the production of secondary electrons in ionization events. In Method 1 the Geant4 kernel was modified. In Method 2 Geant4 was not modified. In both methods a unique flag number assigned to each new split electron was inherited by its progeny, permitting reclassification of the split events as if produced by independent histories.

Computational efficiency and accuracy were evaluated for simulations of 0.5–20 MeV protons and 1–20 MeV/u carbon ions for three endpoints: (1) mean of the ionization cluster size distribution, (2) mean number of DNA single-strand breaks (SSBs) and double-strand breaks (DSBs) classified with DBSCAN, and (3) mean number of SSBs and DSBs classified with a geometry-based algorithm.

For endpoint (1), simulation efficiency was 3 times lower when splitting electrons generated by direct ionization events of primary particles than when splitting electrons generated by the first ionization events of secondary electrons. The latter technique was selected for further investigation. The following results are for Method 2, with relative efficiencies about 4.5 times lower for Method 1. For endpoint (1), relative efficiency at 128 split electrons approached maximum, increasing with energy from 47.2±0.2 to 66.9±0.2 for protons, decreasing with energy from 51.3±0.4 to 41.7±0.2 for carbon. For endpoint (2), relative efficiency increased with energy, from 20.7±0.1 to 50.2±0.3 for protons, 15.6±0.1 to 20.2±0.1 for carbon. For endpoint (3) relative efficiency increased with energy, from 31.0±0.2 to 58.2±0.4 for protons, 23.9±0.1 to 26.2±0.2 for carbon. Simulation results with and without splitting agreed within 1% (2 standard deviations) for endpoints (1) and (2), within 2% (1 standard deviation) for endpoint (3).

In conclusion, standard particle splitting variance reduction techniques can be successfully implemented in Monte Carlo track structure codes.

1 Introduction

In the study of initial damage to DNA from ionizing radiation, the spatial distribution of individual ionization events of charged particles is of particular importance [1]. The Monte Carlo method provides the means to estimate nanodosimetric quantities of interest such as the moments of probability distributions of ionization clusters [2] or the relative yield of single and clustered strand breaks in nanometric scaled geometries [3]. Monte Carlo radiation track-structure codes are available to simulate the transport of electrons and light ions interaction by interaction at nanometric scales [4]. This approach is much more demanding in computer processing time than the more conventional condensed-history Monte Carlo codes that are often used for calculation of dose or fluence distributions in radiotherapy. For such macroscopic calculations, the multitude of individual interactions that typically occur along the path of an energetic charged particle is condensed into an average path-segment or condensed history [5].

Following each and every interaction along a particle track can take considerable time. Techniques are available to speed up the simulation, such as the early termination of the particle track when its kinetic energy reaches a user-defined value [6], or the restriction of interaction-by-interaction tracking of particles to specific regions, with condensed-history tracking performed outside these regions [7]. These approaches can potentially introduce bias to the results, as the contribution of important tracks to the scoring region can be lost due to premature termination of primary particles or failure to generate secondary particles.

Variance reduction techniques (VRTs), by definition, reduce execution time to achieve the same statistical precision without introducing systematic errors into the results. The most widely used VRT is the particle splitting technique (PST), described in more detail in the Methods section, in any of its modalities: uniform [8], selective [9], directional [10], and geometry-based [11][12], among many others, (see, for example, [13] for a summary of VRTs in radiotherapy).

In this work, we explored the use of PSTs in Monte Carlo Track Structure (MCTS) simulations for calculation of nanodosimetric quantities, based on the distribution of ionization events about single tracks. Although PST is well established, the technique was developed to improve the scoring of volume-averaged quantities. Care must be taken to avoid systematic errors when implementing PST in track structure simulations. To our knowledge, this is the first time a variance reduction technique has been implemented and validated for Monte Carlo track-structure simulations for calculating nanodosimetric quantities. A variation of the uniform PST was implemented in the TOPAS-nBio extension of the well-established TOPAS Monte Carlo tool [14] built on the top of Geant4 [15]. The physical processes used were those available in the Geant4-DNA package [16], [17]. A gain in efficiency was anticipated as the moments of the ionization distributions are correlated with radiobiological quantities of high interest, including SSBs and DSBs [18], [19]. We determined the computational efficiency of this technique in the computation of the mean of ionization cluster size distributions and SSBs and DSBs classified with two different scoring approaches. The accuracy of our implementation of PST was validated with reference data generated without PST for protons and carbon with primary energies within the energy range of interest in the Bragg peak of clinical proton and carbon ion beams. As an additional contribution, a new example named “*splitting*” is being developed to be included in the Geant4-DNA examples directory for future release of Geant4.

2 Materials and Methods

2.1 Geant4-DNA and TOPAS-nBio

We used TOPAS v3.0 with an alpha version of the TOPAS-nBio extension [20]. TOPAS and TOPAS-nBio are based on the Geant4-DNA free, open access software. TOPAS is available for download from www.topasmc.org, as of March 9, 2017 having a license fee. The TOPAS-nBio extension is currently under development and is intended to be open-source and freely available by 2019. TOPAS was built on top of Geant4 (version 10.2.p02), therefore all of the TOPAS physics relies on Geant4 capabilities. The physics list in TOPAS can be defined in (but is not restricted to) a modular way by combining the so-called Geant4 physics constructors [14]. This work uses the G4EmDNAPhysics constructor. TOPAS allows use of other options; e.g. G4EmDNAPhysics_option1, etcetera. For example, the Kyriakou et al [21], [22] physics model for low-energy electron transport recently implemented in Geant4-DNA is available in TOPAS using the G4EmDNAPhysics_option4 constructor. In the physics list used in this work, the modeling of energy loss is based on the dielectric response function formalism, which allows the calculation of electronic excitation and ionization cross sections for electrons. The models available in the G4EmDNAPhysics constructor (ionization, vibrational excitation and attachment) are described in the references [17], [23], [24]. Briefly, for electrons these physical models include elastic scattering with the Screened Rutherford model, the Plane-Wave first Born approximation for description of ionization and electronic excitation from 11 eV to 1 MeV, the Møller-Bhabha model for ionization elsewhere, the Sanche model for vibrational excitation and the Melton model for molecular attachment. For protons, the Rudd model for ionization was used up to 2 MeV, whereas the ionization model described in [23] was used elsewhere; the Miller-Green model was used for electronic excitation from 11 eV to 500 keV, the model based on Born theory for energies above this limit, and the charge decrease was modeled with the Dingfelder model. For carbon the Rudd model for ionization was used from 0.5 MeV. Finally, for neutral hydrogen, the Rudd model for ionization, the Miller-Green formula from 11 eV to 500 keV for excitation and the Dingfelder approach for charge increase from 100 eV to 100 MeV were used.

2.2 Flagged uniform particle splitting

A modification of the well-known uniform PST was implemented. The split process was either applied to electrons produced by direct ionization events of primary particles, as illustrated with a simple example in Figure 1, or to electrons produced by ionization events from secondary electrons. Henceforth, these will be called *splitting on primary ionization* and *splitting on first secondary ionization*, respectively. In the latter case, the split process was applied only once per secondary electron at the first ionization from the secondary electron as this represented less complexity in programming and in the classification of the tracks at the final analysis.

In both cases, when a particle experienced an ionization event in a region of interest previously defined by the user, the ionized electron was split into N_S electrons. The statistical weight of the electron was decreased by $1/N_S$, as usually performed in uniform PST [8], *ensuring energy conservation, as the weighted sum of the energy of the split electrons is equal to the energy of the ionized electron*. The energy and momentum of every new electron were resampled accordingly to the corresponding Geant4 process. This split was performed independently of the physical model, that is, once that the ionization event was sampled under some specific physical model, then the split was applied to the ionized electron. Russian Roulette, typically used in combination with PST [8], was included in the following way. If the kinetic energy of the secondary electron was lower than a threshold value then it was either terminated with a residual probability of $1-1/N_S$ or the electron was kept with the statistical weight increased by a factor of N_S.

Special care must be taken in the analysis of track structures when the simulations are modified with the uniform PST. The cluster distribution could be biased as more tracks are produced within the same history, potentially leading to an overestimation of the cluster sizes due to the contribution of ionizations from new tracks as shown in Figure 1. In this idealized PST example, a primary charged particle traverses a double strand of DNA. An ionization event occurs and the secondary electron causes a single strand break (SSB) on one of the strands. The secondary electron is split into two additional electrons, one of these adding an extra SSB on the opposite strand. With SSB's on opposing strands and separated by a distance of less than 10 base pairs, a DSB could be erroneously counted. Thus with PST, care must be taken to properly count the resulting number of SSBs and DSBs per primary particle.

To overcome this problem, a method was implemented that assigns a new virtual property to the split particle. A flag containing the split track identification number `SplitTrackID` was assigned to each new split electron, and inherited by all progeny (every particle generated or set in motion by the split electron). The default value was set to 1 and only particles with a `SplitTrackID` equal to 1 at ionization events were split.

At each splitting event, the flag associated with each new split electron was assigned an integer value from 3 to N_S+2. If the ionizing incoming particle was an electron, its corresponding `SplitTrackID` was set to 2 to distinguish it from electrons that were not split. If the incoming ionizing particle was a proton or a carbon ion, its `SplitTrackID` was kept equal to 1. This assignment allowed limiting the split to only once in the case of ionizations caused by electrons and allowed a split at every ionization event for protons or carbon.

Example tracks of a primary proton and its secondary electrons produced by ionization events are shown in Figure 2. On the left side of the figure, the split process was applied to the proton ionization process. In this example, the split process occurs at the ionization event of the primary proton at around z = 4 nm, producing three new electrons. On the right side, the split process was applied to the electron ionization process. As shown, a secondary electron set in motion by the proton (close to z = 0 nm) moves in the −x direction about 2 nm where the first ionization event of this electron invokes the split process, producing three new electrons.

When additional electrons were produced by a split electron further along its track, the `SplitTrackID` of this electron was inherited by all its progeny with no additional splitting. This flag allowed reclassification of the split events as if they were produced by independent histories. As an important note, for the final analysis, the contribution of the primary proton (and the first ionization of the secondary electron when splitting on first secondary ionization, see Figure 2) must be added to every scorer flagged with the `SplitTrackID` at the completion of the simulation of each history.

The use of Russian roulette combined with PST is a common practice in variance reduction for radiotherapy simulations. In this work, however, Russian roulette did not improve the efficiency (results not shown). That is, the penalty time to perform Russian roulette resulted in no reduction in execution time for the same statistical precision. In addition, significant bias was introduced into the results when the threshold energy to apply Russian roulette was increased. Thus, the final implementation of PST was done without Russian roulette.

2.3 Computational efficiency and validation

2.3.1 Scoring metrics and statistical uncertainty calculation—Two biologically meaningful quantities of interest in nanodosimetry are the first moment $M_1(Q)$ and the cumulative distribution $F_2(Q)$ of the ionization cluster size distribution $P(\nu|Q)$ produced by a particle beam of quality Q (see [2] [19] for more details). The cluster size ν is the number of ionizations produced within the scoring region by a single history [2]. The corresponding expressions for $M_1(Q)$ and $F_2(Q)$ are:

$$M_1(Q)=\sum_{\nu=0}^{\infty}\nu P(\nu|Q),\;\; F_2(Q)=\sum_{\nu=2}^{\infty}P(\nu|Q). \tag{1}$$

The quantities defined in Equation 1 were used to validate the variance-reduced simulations by comparing those results with data produced by reference simulations without PST (N_s=1). A different approach was used for SSB and DSB calculations, with the corresponding probability distributions obtained and analogous expressions to Equation 1 used, but in this case using the number of SSBs or DSBs per history, instead of the quantity ν.

To calculate the statistical uncertainty S_x, we used the second moment of the probability distribution $P(\nu|Q)$ divided by the number of scored events and took the square root of this quantity. This method was performed for each of 12 statistically independent simulations (using different random seeds), and the average value of the statistical uncertainty was obtained.

Finally, the computational efficiency ε of the Monte Carlo simulations was calculated with:

$$\varepsilon = \frac{1}{S_x^2 T}, \quad (2)$$

where T is the average execution time of the 12 simulations in seconds. As S_x is associated with a dimensionless quantity (mean cluster size, mean SSB or mean DSB) the unit of the efficiency is s^{-1}.

The efficiency of PST using Method 1 and Method 2 was evaluated for representative simulations in nanodosimetry. The estimation of ionization distributions is described in the previous section. Complementary simulations for the estimation of SSB and DSB distributions classified with the DBSCAN algorithm and a geometry-based algorithm are described in the following two sections.

2.3.2 Use case: Ionization cluster size distributions—Ionization cluster size distributions produced by monoenergetic protons of 0.5, 1, 5, 10, and 20 MeV and carbon ions of 1, 5, 10, and 20 MeV/u were simulated normally incident on the midpoint of the curved surface of a homogeneous water cylinder of 5 nm diameter and 10 nm length. The use of a single angle of incidence was arbitrary. The dimensions of the cylinder have been proposed by others to estimate nanodosimetric track structure parameters in [25], [26]. The cylinder was centered in a cubic water phantom of 150×150×150 nm^3. The particle split was restricted to those events occurring in the cylindrical region. For carbon, the particle split was applied only to the electron ionization process, as discussed below. Reference data was generated by simulating at least 1.5×10^5 and 5×10^4 histories for proton and carbon (for the lowest energies), respectively; whereas final simulations with PST required at least 1000 histories for proton and carbon, respectively.

2.3.3 Use case: Single and double strand break yields—A complementary study of efficiency was performed for the estimation of SSB and DSB yields for several source energies in two scenarios. Again, the particle split was restricted to the scoring region.

In the first scenario, reference data was generated for SSB and DSB (without PST) for a mono-energetic and mono-directional point source of protons of 0.5, 1, 5, 10 and 20 MeV and carbon ions of 1, 5, 10 and 20 MeV/u, incident on the upstream surface of a water box of 1×1×0.5 μm^3. The water box was centered in a water cube of 2×2×2 μm^3. DNA is not present in the simulation. The SSBs and DSBs were estimated in the smaller phantom with the DBSCAN algorithm which is described in [27] and currently included in the extended examples of Geant4 (in the example named clustering [16]. The parameters for DBSCAN were a maximum distance of 3.4 nm, a threshold linear energy distribution from 5 eV to 37.5 eV to define an SSB and a minimum of two SSBs to create a DSB [27]. Reference data was generated by simulating at least 10^5 and 10^4 histories for proton and carbon (for the lowest energies), respectively; whereas final simulations with PST required at least 5000 and 1000 histories for proton and carbon, respectively.

In the second scenario, for the same energies as in the first scenario, the SSB and DSB were classified as described in [28] by using the geometrical information of models from the Protein Data Bank database [29]. In this work, a model named pdb4dna was used. This model represents a tetranucleosome. The scoring region was limited to a box of 4.85×7.61×12.6 nm^3 (to 3 significant figures) embedded in a water cube of 50×50×50 nm^3. The scoring region was irradiated with particles starting from points randomly distributed in a uniform distribution on the surface of a spherical shell with a 12.6 nm^3 radius and directed into the sphere in random directions in a uniform distribution. A minimum energy of 8.22 eV was required to form an SSB, and a DSB required at least 2 SSB's within 10 base pairs [28]. Reference data was generated by simulating at least 10^6 and 1.2×10^5 histories for proton and carbon (for the lowest energies), respectively; whereas final simulations with PST required at least 5000 and 1000 histories for proton and carbon, respectively.

These two examples, available in release version 10.2 patch 02 of Geant4-DNA, were implemented in TOPAS-nBio by adding two new scorers, dbscan and pdb4dna, that can be attached to any geometry for future simulations. The reference simulations shown are for efficiency estimation purposes only. They do not constitute a benchmark comparison.

3 Results

3.1 Cluster size distributions

3.1.1 Protons—The dependence of the efficiency on N_S (incremented in powers of 2) for the estimation of the mean (first moment) of cluster size distributions is shown in Figure 3 for five proton energies. Results comparing Method 1 (Geant4 kernel modified, see section 2.2.1) and Method 2 (Geant4 not modified) for PST splitting on primary ionization are shown in the graph on the left. Results comparing Methods 1 and 2 for PST splitting on first secondary ionization are shown in the graph on the right. In both cases, efficiency increased with increasing energy and increasing N_S, up to 128 split electrons where the efficiency approaches a maximum at all energies simulated. When splitting on primary ionization, with $N_S = 128$, the relative efficiency (the ratio of efficiency between $N_S = 128$ and $N_S = 1$) for Method 2 increased by a factor of 12.4±0.1 at 0.5 MeV up to a factor of 21.8±1.0 at 20 MeV (similar values for Method 1). Splitting on the first secondary ionization resulted in an about 3 times higher relative efficiency with PST. Using Method 2, the efficiency reached a maximum at $N_S = 128$, the relative efficiency increasing by a factor of 47.2±0.2 (31.0±0.1 for Method 1) at 0.5 MeV up to a factor of 66.9±0.2 (59.1±0.4 for Method 1) at 20 MeV. In this latter case, the efficiency starts decreasing for larger values of N_S.

In both Methods 1 and 2, the results when using PST agreed with the reference simulation results for all energy values within 1% (within 0.2% statistical uncertainty, one standard deviation) for the $M_1(Q)$ and $F_2(Q)$ distributions calculated with Equation 1. The accuracy of PST with $N_S = 128$ for Method 2 is shown in Figure 4 (Method 1 results are not shown).

3.1.2 Carbon ions—The efficiency of the flagged uniform PST on first secondary ionization for ionization distributions produced with carbon is shown on the left side of Figure 5. The relative efficiency for PST implemented with Method 2 at N_S of 128, close to the maximum, was 51.3±0.4 for 1 MeV/u, 47.5±0.3 for 5 MeV/u, 44.4±0.2 for 10 MeV/u and 41.7±0.2 for 20 MeV/u.

The graph on the right side of Figure 5 shows the probability distributions of ionization cluster size for the reference simulations and the variance-reduced simulations with N_s = 128. For each of the energies the reference and PST simulations were run for approximately the same execution time. The reference data was calculated with sufficient statistical precision to validate the accuracy of PST in reasonable run times. The fractional uncertainty per bin for the distribution corresponding to 1 MeV/u is shown in the inset. Simulations with PST were run to achieve a much better statistical uncertainty than the reference data. The accuracy in $M_1(Q)$ and $F_2(Q)$ was confirmed within 1 standard deviation of the reference data.

3.2 Single and double strand break classification with the DBSCAN algorithm

All results of this section were obtained with PST implemented on the first secondary ionization. Since splitting on the first secondary ionization using Method 1 was much less efficient than Method 2 for the SSB and DSB use cases, and accuracy from the two methods was comparable for the cluster size distribution use case, accuracy validation for these cases was based solely on Method 2.

3.2.1 Protons—The efficiency of estimating the mean number of DSBs, with the DBSCAN algorithm implemented as a scorer in TOPAS-nBio, is shown on the left side of Figure 6. The efficiency gain is close to saturation for PST with Method 1 from N_s = 32 whereas it continues to increase beyond this point for PST with Method 2. For the latter setup, at Ns = 128, efficiency gains from 20.7 ±0.1 at 0.5 MeV to 50.2 ±0.3 at 20 MeV were achieved. The graph on the right side of Figure 6 shows mean SSB and DSB for energies ranging from 0.5 to 20 MeV. The PST result agreed with the reference simulations within 1% (statistical uncertainty of 0.5% or less, 1 standard deviation).

3.2.2 Carbon ions—Figure 7 shows the efficiency for DSB estimation with carbon in water. For all energies, the gains in the efficiency drop off with increasing values of N_s and approach saturation with N_s larger than 32 for PST implemented with Method 1, whereas they continue to increase beyond this point for PST implemented with Method 2. For the latter setup, at Ns = 128, the efficiency improvement of factors from 15.6 ±0.1 to 20.2 ±0.1 were achieved for 1 MeV/u and 20 MeV/u, respectively. Figure 7 also shows the mean values of DSB and SSB as a function of energy for reference and variance-reduced (N_s = 128) simulations. The maximum differences were below 0.5% (within statistical uncertainty of 0.5%, 1 standard deviation) for all energies.

3.3 Single and double strand break classification based on geometry

3.3.1 Protons—The efficiency with respect to N_s for DSBs classified with a geometry-based algorithm [28] is shown on the left side of Figure 8. The relative efficiency ranges from a factor of 31.0 ±0.2 up to a factor 58.2 ±0.4 for N_s = 128. For energies of 5 MeV or higher, the efficiency continues to increase with increasing N_s, whereas for lower energies the efficiency nearly saturates at this point. The mean SSB and DSB values for energies from 0.5 to 20 MeV are also shown on the right side of Figure 8 for both the reference and variance reduced simulations with N_S = 128. The mean number of SSBs agreed within 2% for all energies (statistical uncertainty below 1%). The mean number of DSBs agreed within 3% at 10 MeV and below (statistical uncertainty of 2.5% or less), and within 7% at 20 MeV (statistical uncertainty of 4%).

3.3.2 Carbon ions—For carbon, the efficiency variation with respect to N_S is shown in Figure 9. The relative efficiency goes from 23.9 ±0.1 at 1 MeV/u to 26.2 ±0.2 at 20 MeV/u with N_S = 128, a modest increase in relative efficiency with increasing energy. The mean number of SSBs and DSBs for the reference simulations is compared to those for the variance-reduced simulations on the right side of Figure 9. The differences were within of 2% for the mean number of SSBs (statistical uncertainties lower than 0.5%), and within 2% for the mean number of DSBs (statistical uncertainties of 1% or less).

4 Discussion

The flagged uniform PST implemented in TOPAS-nBio resulted in large efficiency gains without loss of accuracy. The necessity of propagating the flag from particles to their progeny was fulfilled with two methods. Method 1 involved a modification to the Geant4 kernel. Method 2 involved the implementation of auxiliary classes without a modification of Geant4. Method 2 led to much higher efficiency gains than Method 1 when splitting on the first secondary ionization. Although the flag was updated in the particle splitting process in both methods, in Method 2 the flag was only propagated when a new particle was created, whereas in Method 1 the flag was propagated at the creation of a new particle and at every step of every particle, requiring many more operations and thus more execution time.

On the other hand, efficiency gains with Methods 1 and 2 were comparable when splitting on the primary ionization. As primary ionizations are more frequent events compared with secondary ionizations (about 8.5% more for 0.5 MeV protons, 34% for 20 MeV protons, 6.5% more for 1 MeV/u, and 19% more for 20 MeV/u carbon ions in the examples of section 3.1.1 and 3.1.2, respectively), splitting primary ionizations in Method 2 requires more operations than splitting on the first secondary ionization, increasing execution time that led to efficiency gains comparable to Method 1. In the same way, particle splitting on primary ionization was less efficient than splitting on the first secondary ionization. The use of the particle splitting with the new model from [21], [22] may show higher relative efficiency gains (a factor of ~1.5) due to the much smaller ionization yield than obtained with the previous physics model.

Efficiency gains were achieved with protons and carbon in the energy range of interest in the Bragg peak of clinical proton and carbon ion beams for all three cases of nanometer-scale simulation considered. The efficiency gains in the calculation of nanodosimetric quantities of interest varied with the complexity of the application for proton and carbon ions and also varied with energy for proton beams (Figure 10). For proton sources, higher efficiency gains were achieved with larger energies (over 5 MeV) in all cases due to the sparse ionization patterns produced at these energies. Increasing the number of secondary electrons in the particle history by means of the split technique resulted in a large increase in the number of ionizations events in the higher energy proton track, leading to a reduced variance without a correspondingly large increase in simulation time. On the other hand, for high LET protons (lower energies), the additional time required to transport the new particles was enough to impact the efficiency gain, with the efficiency saturating at lower values of N_S than the lower LET (higher energy) protons. For the energy range in this study, carbon has a higher LET than protons, as shown on the left side of Figure 10. Carbon with the lowest LET simulated in this study produced more ionization from primaries (carbon) than from secondaries (electrons) as discussed earlier. This leads to a relative efficiency similar to or slightly less than that for the highest LET protons in the study.

The relative efficiency is degraded with increasing complexity of the scoring technique as shown for both protons and carbon in Figure 10. In this work, the DBSCAN algorithm had a higher complexity than the other two algorithms. DBSCAN performs operations on data stored in arrays, using re-sampling in deposited energy and sorting operations to find ionization events spatially close enough to one to another to form clusters from the full set of ionization event locations scored during a particle history [30], [31]. The array size increases with N_S, dramatically increasing execution time compared with particle tracking or the scoring of ionization events. The geometry-based classification algorithm, on the other hand, resulted in a more efficient way to estimate SSB and DSB values, as no further re-sampling or complex sorting is performed after the transport of a single history [28]. The algorithm used to create cluster size distributions led to the highest efficiency gains and was the least complex, only requiring the storage of ionization events along the particle track.

Further improvement in efficiency can be achieved by restricting the use of MCTS codes to regions of interest while performing condensed-history Monte Carlo elsewhere [7]. This method performs best when the volume of the region of interest is much smaller than the container volume. For example, for the DBSCAN results shown in Figure 6, after restricting the MCTS transport to the scoring region, an improvement in efficiency is achieved as shown for protons in Figure 11. However, as N_S increases, the higher number of particles in the scoring region (where the split occurs) increases the execution time, reducing the efficiency. Efficiency may be further enhanced by combining splitting on primary ionization and first secondary ionization and possibly by splitting all ionization events. However, we chose to limit PST in this study to single ionizations on each track due to the much higher complexity in implementation and processing of multiple splits.

The Geant4 pdb2dna algorithm we used to estimate the number of DNA strand breaks was restricted to simple SSB's and DSB's [28]. We expect our demonstration of the performance of PST in this scenario will motivate further exploration of the capabilities of these kinds of techniques in more complex scenarios.

From Geant4 version 9.6, Geant4-DNA may be used to simulate the pre-chemical and chemical stages of water radiolysis [32], [33]. In this case we expect the distribution of radiolytic species to be unaffected by use of PST when the flag is used to produce the same weighted number of different radiolytic species. The study of PST in such scenarios needs to produce the correct weighted number of each of the radiolytic species at: 1) the pre-chemical stage, with the number of radiolytic species produced separated per split particle by using the flag assigned at the splitting event, and 2) at the chemical stage, restricting the reaction between species to tracks of the same flag. However, this may prove impractical as the addition of new chemical tracks from the split particles will increase the already computationally high demand on CPU time of the chemical stage.

5 Conclusions

The variance reduction techniques applied in this work can provide significant gains in computational efficiency for Monte Carlo track structure codes without compromising accuracy. Splitting the electrons set in motion by primary particles in an ionization event proved to be less efficient than splitting the electrons set in motion by secondary electrons for only the first ionization event along the secondary electron track. The gain in efficiency in this latter case depended on the complexity of the scored quantity, offering a larger gain for less complex scoring methods. It also depended on the energy or LET of the particle of interest, providing a larger gain for low-LET, high-energy particles. Efficiency approached maximum near 128 split electrons for all use cases simulated with split on the first secondary ionization, with efficiency gains of 21–67 for 1–20 MeV protons, 16–51 for 1–20 MeV/u carbon ions. The PST implementation we used applies to all physics models available in the underlying Geant4, although use of different physics models may affect the efficiency gain.

These techniques have been provided in TOPAS starting with version 3.1. Both the TOPAS release and the Geant4 example named "*splitting*" under development use the second method described in the Methods section.

Acknowledgments

This work was supported by National Cancer Institute Grants 1R01CA187003 and 1P20CA183640.

Appendix

Implementation

PST was implemented in TOPAS-nBio by using a concrete class based on the `G4WrapperProcess` class that allows biasing of a specific physical process. Prior to that, a special function is required to setup and inherit the `SplitTrackID` in the tracking process of Geant4. We implemented that function in two ways as described below.

The first method (hereafter referred to as Method 1), involved modification of the Geant4 kernel by introducing two functions based on the standard Geant4 functions `GetWeight()` and `SetWeight()`. These functions propagate the statistical weight along the particle tracking; they return a double precision value. Analogous to these, we implemented the `GetSplitTrackID()` and `SetSplitTrackID()` functions. At the beginning of the simulation, the `SetSplitTrackID()` assigns a `SplitTrackID` value equal to 1 (integer) to every primary particle. This number is updated at the time the split process is performed and is propagated by the Geant4 transporting functions. Thus, the `SplitTrackID` can be accessed at any time with objects of the `G4StepPoint` or `G4Track` classes.

The second method to implement the functions (hereafter referred to as Method 2), is based on a class inherit from the abstract class `G4VUserTrackInformation` and one based on the class `G4UserTrackingAction`. The `SplitTrackID` is set in the method `G4UserTrackingAction::PreUserTrackingAction()` and propagated to the progeny in the `G4UserTrackingAction::PostUserTrackingAction()` (see [34]). The value is updated in the concrete class based on `G4WrapperProcess` that performs the split particle process, as in the Method 1. Code 1 shows the main part of the code that performs the split process implementation and the updating of the `splitTrackID` value with Method 2.

References

1. Goodhead DT. Initial events in the cellular effects of ionizing radiations: clustered damage in DNA. Int. J. Radiat. Biol. 1994; 65(1):7–17. [PubMed: 7905912]
2. Grosswendt B, Pszona S. The track structure of alpha-particles from the point of view of ionization-cluster formation in 'nanometric' volumes of nitrogen. Radiat Env. Biophys. 2002; 41(2):91–102. [PubMed: 12201061]
3. Nikjoo H, O'Neill P, Goodhead DT, Terrissol M. Computational modelling of low-energy electron-induced DNA damage by early physical and chemical events. Int. J. Radiat. Biol. 1997; 71(5):467–483. [PubMed: 9191891]
4. Nikjoo H, Uehara S, Emfietzoglou D, Cucinotta FA. Track-structure codes in radiation research. Radiat. Meas. 2006; 41(9–10):1052–1074.
5. Berger, MJ. Monte Carlo calculation of the penetration and diffusion of fast charged particles. In: Alder, B.Fernbach, S., Rotenberg, M., editors. Methods in Computational Physics. Vol. 1. New York: Academic Press; 1963. p. 135
6. Bielajew, AF., Rogers, DWO. Variance-reduction techniques. In: Jenkins, TM.Nelson, WR., Rindi, A., editors. Monte Carlo transport of electrons and photons. Ettore Majorana International Science Series; 1988. p. 407
7. Ivanchenko V, Apostolakis J, Bagulya a, Abdelouahed HB, Black R, Bogdanov a, Burkhard H, Chauvie S, Cirrone P, Cuttone G, Depaola G, Di Rosa F, Elles S, Francis Z, Grichine V, Gumplinger P, Gueye P, Incerti S, Ivanchenko a, Jacquemier J, Lechner a, Longo F, Kadr O, Karakatsanis N, Karamitros M, Kokoulin R, Kurashige H, Maire M, Mantero a, Mascialino B, Moscicki J, Pandola L, Perl J, Petrovic I, Ristic-Fira a, Romano F, Russo G, Santin G, Schaelicke a, Toshito T, Tran H, Urban L, Yamashit T, Zacharatou C. Recent Improvements in Geant4 Electromagnetic Physics Models and Interfaces. 3th Monte Carlo Conf. MC2010. 2011; 2:898–903.
8. Rogers DWO, Faddegon B, Ding GX, Ma C-M, We J. BEAM: A Monte Carlo code to simulate radiotherapy treatment units. Med. Phys. 1994; 22(5):503–524.
9. Sheikh-Bagheri, D. Monte Carlo study of photon beams from medical linear accelerators: Optimization, benchmark and spectra. Carleton University; 1998.
10. Kawrakow I, Rogers DWO, Walters BRB. Large efficiency improvements in BEAMnrc using directional bremsstrahlung splitting. Med. Phys. 2004; 3110:2883. [PubMed: 15543798]
11. García-Pareja S, Vilches M, Lallena AM. Ant colony method to control variance reduction techniques in the Monte Carlo simulation of clinical electron linear accelerators of use in cancer therapy. Journal of Computational and Applied Mathematics. 2010; 233(6):1534–1541.
12. Wagner JC, Haghighat A. Automated Variance Reduction of Monte Carlo Shielding Calculations Using the Discrete Ordinates Adjoint Function. Nucl. Sci. Eng. 1998; 128:186–208.
13. Fippel, M. Variance reduction techniques. In: Seco, J., Verhaegen, F., editors. Monte Carlo Techniques in Radiation Therapy. CRC Press; 2013. p. 29
14. Perl J, Shin J, Faddegon B, Paganetti H. TOPAS: An innovative proton Monte Carlo platform for research. Med. Phys. Nov.2012 39:6818–6837. [PubMed: 23127075]
15. Agostinelli S, Allison J, Amako K, Apostolakis J, Araujo H, Arce P, Asai M, Axen D, Banerjee S, Barrand G, Behner F, Bellagamba L, Boudreau J, Broglia L, Brunengo a, Burkhardt H, Chauvie S, Chuma J, Chytracek R, Cooperman G, Cosmo G, Degtyarenko P, Dell'Acqua a, Depaola G,

Dietrich D, Enami R, Feliciello a, Ferguson C, Fesefeldt H, Folger G, Foppiano F, Forti a, Garelli S, Giani S, Giannitrapani R, Gibin D, Gómez Cadenas JJ, González I, Gracia Abril G, Greeniaus G, Greiner W, Grichine V, Grossheim a, Guatelli S, Gumplinger P, Hamatsu R, Hashimoto K, Hasui H, Heikkinen a, Howard a, Ivanchenko V, Johnson a, Jones FW, Kallenbach J, Kanaya N, Kawabata M, Kawabata Y, Kawaguti M, Kelner S, Kent P, Kimura a, Kodama T, Kokoulin R, Kossov M, Kurashige H, Lamanna E, Lampén T, Lara V, Lefebure V, Lei F, Liendl M, Lockman W, Longo F, Magni S, Maire M, Medernach E, Minamimoto K, Mora de Freitas P, Morita Y, Murakami K, Nagamatu M, Nartallo R, Nieminen P, Nishimura T, Ohtsubo K, Okamura M, O'Neale S, Oohata Y, Paech K, Perl J, Pfeiffer a, Pia MG, Ranjard F, Rybin a, Sadilov S, Di Salvo E, Santin G, Sasaki T, Savvas N, Sawada Y, Scherer S, Sei S, Sirotenko V, Smith D, Starkov N, Stoecker H, Sulkimo J, Takahata M, Tanaka S, Tcherniaev E, Safai Tehrani E, Tropeano M, Truscott P, Uno H, Urban L, Urban P, Verderi M, Walkden a, Wander W, Weber H, Wellisch JP, Wenaus T, Williams DC, Wright D, Yamada T, Yoshida H, Zschiesche D. Geant4—a simulation toolkit. Nucl. Instruments Methods Phys. Res. Sect. A Accel. Spectrometers, Detect. Assoc. Equip. Jul; 2003 506(3):250–303.

16. Bernal MA, Bordage MC, Brown JMC, Davídková M, Delage E, El Bitar Z, Enger SA, Francis Z, Guatelli S, Ivanchenko VN, Karamitros M, Kyriakou I, Maigne L, Meylan S, Murakami K, Okada S, Payno H, Perrot Y, Petrovic I, Pham QT, Ristic-Fira A, Sasaki T, Štěpán V, Tran HN, Villagrasa C, Incerti S. Track structure modeling in liquid water: A review of the Geant4-DNA very low energy extension of the Geant4 Monte Carlo simulation toolkit. Phys. Med. Dec; 2015 31(8):861–74. [PubMed: 26653251]

17. Incerti S, a Ivanchenko, Karamitros M, a Mantero, Moretto P, Tran HN, Mascialino B, Champion C, Ivanchenko VN, a Bernal M, Francis Z, Villagrasa C, Baldacchin G, Guèye P, Capra R, Nieminen P, Zacharatou C. Comparison of GEANT4 very low energy cross section models with experimental data in water. Med. Phys. 2010; 37(9):4692–4708. [PubMed: 20964188]

18. Grosswendt B, Pszona S, Bantsar A. New descriptors of radiation quality based on nanodosimetry, a first approach. Radiat. Prot. Dosimetry. 2007; 126(1–4):432–444. [PubMed: 17496299]

19. Palmans H, Rabus H, Belchior AL, Bug MU, Galer S, Giesen U, Gonon G, Gruel G, Hilgers G, Moro D, Nettelbeck H, Pinto M, Pola A, Pszona S, Schettino G, Sharpe PHG, Teles P, Villagrasa C, Wilkens JJ. Future development of biologically relevant dosimetry. Br. J. Radiol. 2015; 88:1045.

20. McNamara A, Geng C, Turner R, Mendez JR, Perl J, Held K, Faddegon B, Paganetti H, Schuemann J. Validation of the radiobiology toolkit TOPAS-nBio in simple DNA geometries. Phys. Medica. Jan.2017 33:207–215.

21. Kyriakou I, Šefl M, Nourry V, Incerti S. The impact of new Geant4-DNA cross section models on electron track structure simulations in liquid water. J. Appl. Phys. May.2016 119(19):194902.

22. Kyriakou I, Incerti S, Francis Z. Technical Note: Improvements in geant 4 energy-loss model and the effect on low-energy electron transport in liquid water. Med. Phys. Jun; 2015 42(7):3870–3876. [PubMed: 26133588]

23. Francis Z, Incerti S, Karamitros M, Tran HN, Villagrasa C. Stopping power and ranges of electrons, protons and alpha particles in liquid water using the Geant4-DNA package. Nucl. Instruments Methods Phys. Res. Sect. B Beam Interact. with Mater. Atoms. 2011; 269(20):2307–2311.

24. Villagrasa C, Francis Z, Incerti S. Physical models implemented in the GEANT4-DNA extension of the GEANT-4 toolkit for calculating initial radiation damage at the molecular level. Radiat. Prot. Dosimetry. Feb; 2011 143(2–4):214–218. [PubMed: 21186212]

25. Nikjoo H, Goodhead DT. Track structure analysis illustrating the prominent role of low-energy electrons in radiobiological effects of low-LET radiations. Phys. Med. Biol. 1991; 36(2):229–238. [PubMed: 2008448]

26. Grosswendt B. Formation of ionization clusters in nanometric structures of propane-based tissue-equivalent gas or liquid water by electrons and α-particles. Radiat. Environ. Biophys. 2002; 41(2):103–112. [PubMed: 12201053]

27. Francis Z, Villagrasa C, Clairand I. Simulation of DNA damage clustering after proton irradiation using an adapted DBSCAN algorithm. Comput. Methods Programs Biomed. 2011; 101(3):265–270. [PubMed: 21232812]

28. Delage E, Pham QT, Karamitros M, Payno H, Stepan V, Incerti S, Maigne L, Perrot Y. PDB4DNA: Implementation of DNA geometry from the Protein Data Bank (PDB) description for Geant4-DNA Monte-Carlo simulations. Comput. Phys. Commun. 2015; 192:282–288.

29. Bernstein FC, Koetzle TF, Williams GJB, Meyer EF, Brice MD, Rodgers JR, Kennard O, Shimanouchi T, Tasumi M. The protein data bank: A computer-based archival file for macromolecular structures. Arch. Biochem. Biophys. 1978; 185(2):584–591. [PubMed: 626512]

30. Tran TN, Drab K, Daszykowski M. Revised DBSCAN algorithm to cluster data with dense adjacent clusters. Chemom. Intell. Lab. Syst. 2013; 120:92–96.

31. Francis Z, Incerti S, Ivanchenko V, Champion C, Karamitros M, a Bernal M, El Bitar Z. Monte Carlo simulation of energy-deposit clustering for ions of the same LET in liquid water. Phys. Med. Biol. 2011; 57(1):209–224.

32. Karamitros M, Mantero A, Incerti S, Friedland W, Baldacchino G, Barberet P, Bernal M, Capra R, Champion C, El Bitar Z, Francis Z, Gueye P, Ivanchenko A, Ivanchenko V, Kurashige H, Mascialino B, Moretto P, Nieminen P, Santin G, Seznec H, Tran HN, Villagrasa C, Zacharatou C. Modeling Radiation Chemistry in the Geant4 Toolkit. Prog. Nucl. Sci. Technol. 2011; 2:503–508.

33. Karamitros M, Luan S, Bernal MA, Allison J, Baldacchino G, Davidkova M, Francis Z, Friedland W, Ivantchenko V, Ivantchenko A, Mantero A, Nieminem P, Santin G, Tran HN, Stepan V, Incerti S. Diffusion-controlled reactions modeling in Geant4-DNA. J. Comput. Phys. 2014; 274:841–882.

34. Collaboration G. Geant4 User's Guide for Application Developers. 2015

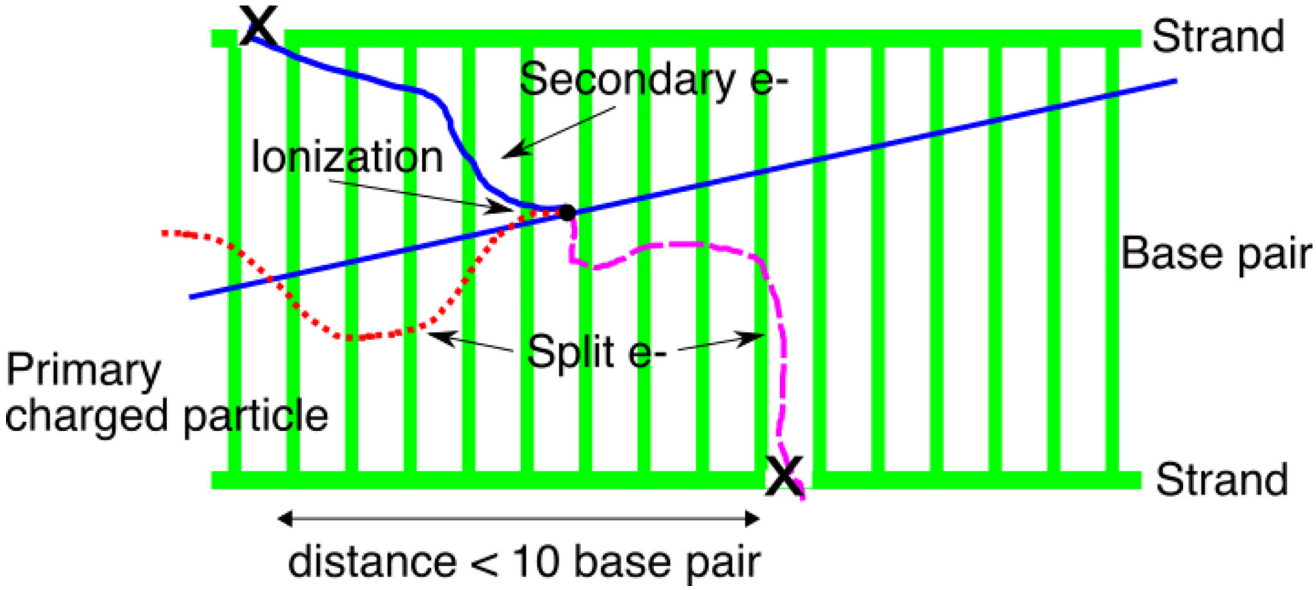

Figure 1.

An idealized scenario of strand-break induction by ionizing particles. Particle splitting occurs at the ionization event. The resulting tracks of the primary charged particle, the original secondary electron (solid line) and the tracks of the two split electrons (dotted and dashed lines) produce DNA breaks (X) in this illustrative case (see text).

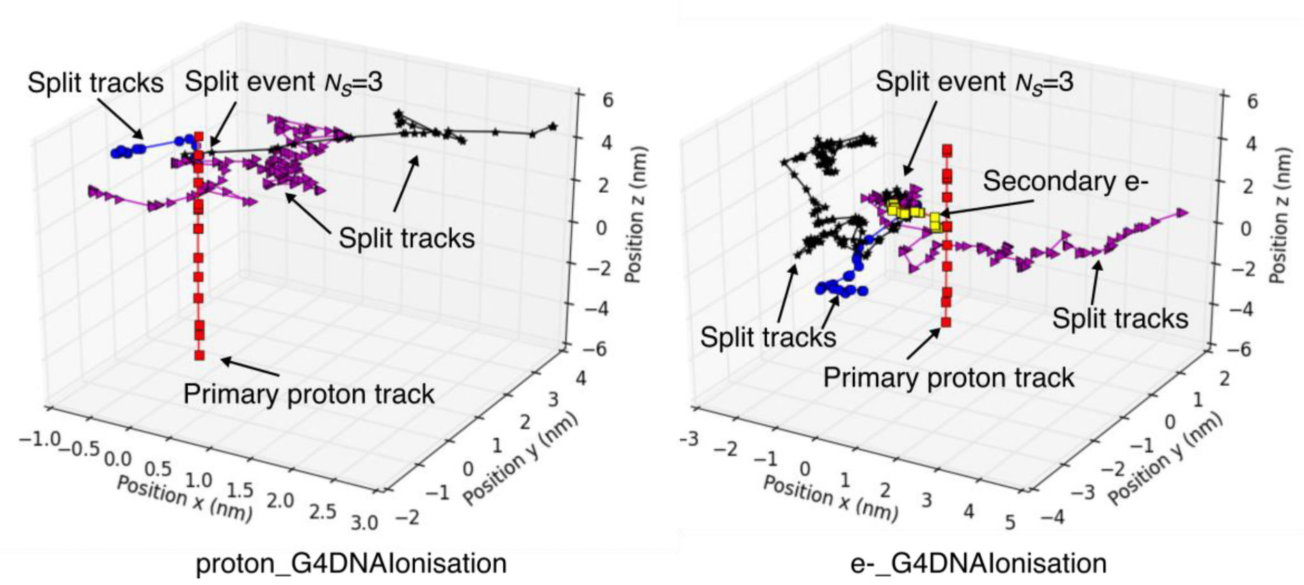

Figure 2.

Examples of simulated tracks initiated by a 0.5-MeV primary proton moving vertically upwards (red) with flagged uniform PST with Ns = 3 (unsplit secondary electron SplitTrackID equal to 2 - yellow, split electrons with SplitTrackID equal to 3 - blue, 4 - black, 5 - magenta). The graph shows two scenarios: Track splits at ionization event produced by the primary proton (left) and track splits at first ionization event produced by the secondary electron (right). Only one proton ionization event is shown for clarity.

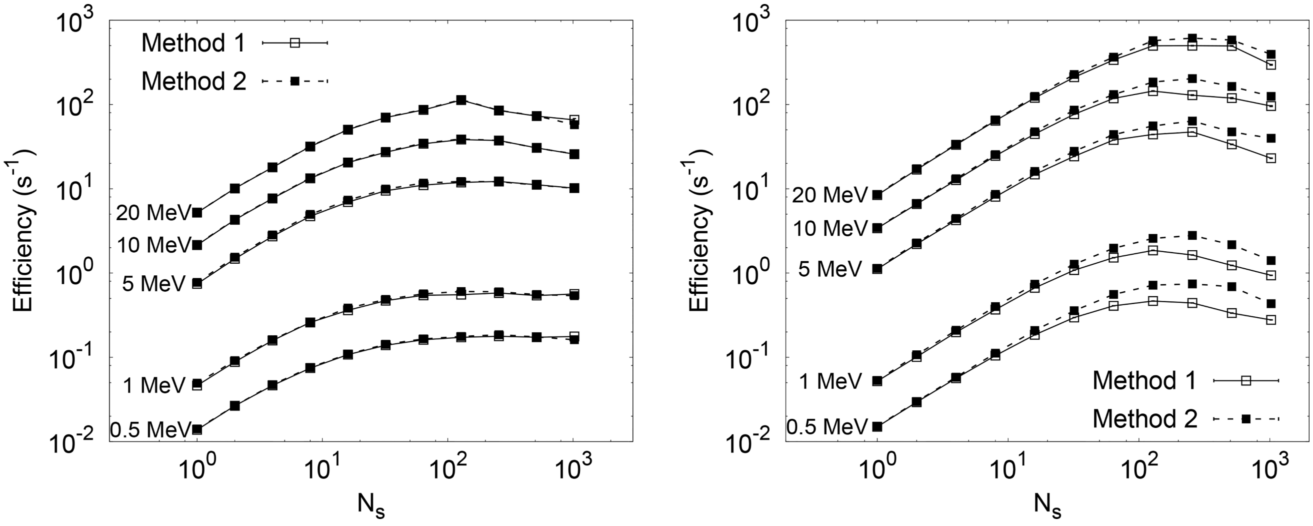

Figure 3.

Efficiency variation in cluster size simulation with N_s for 0.5–20 MeV protons for both Methods 1 and 2 when applied to split on primary ionization (graph on left) and applied to split on first secondary ionization (graph on right). The maximum efficiency is about 3 times larger when splitting on first secondary ionization. The statistical uncertainty was well within the size of the markers.

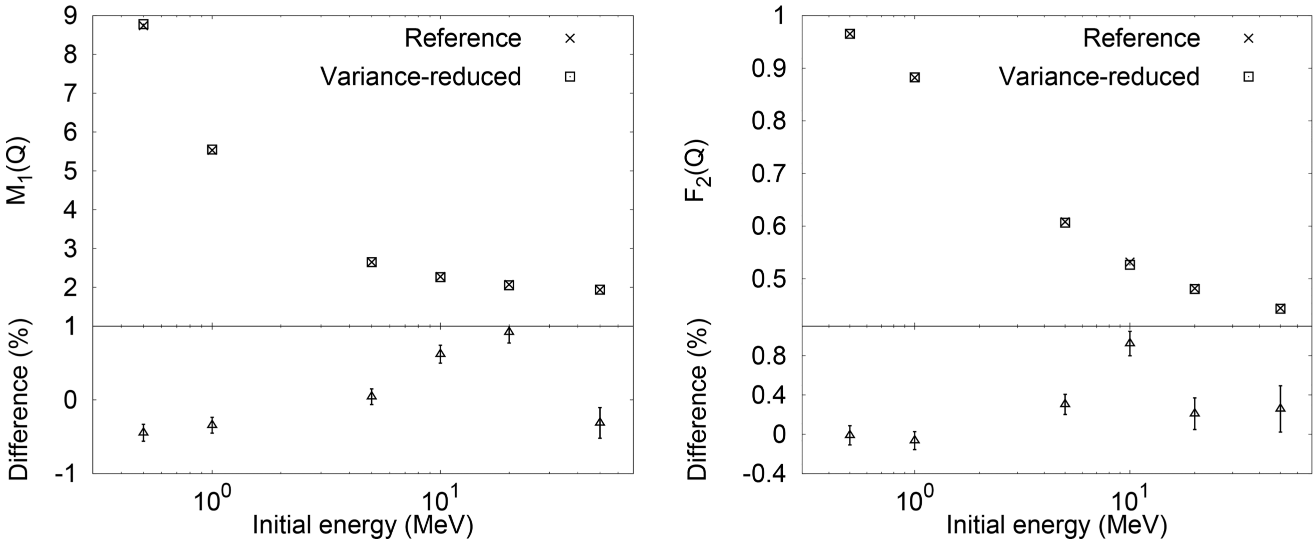

Figure 4.

Validation of splitting on the first secondary ionization using Method 2. First moment $M_1(Q)$ (left) and cumulative distribution $F_2(Q)$ (right) of $P(\nu|Q)$ shown as a function of the proton energy for the two physical processes for reference simulations and for simulations using the flagged uniform PST with $N_s = 128$. The relative difference between PST and reference results is also shown (empty triangles). The error bars on the relative difference represent one standard deviation.

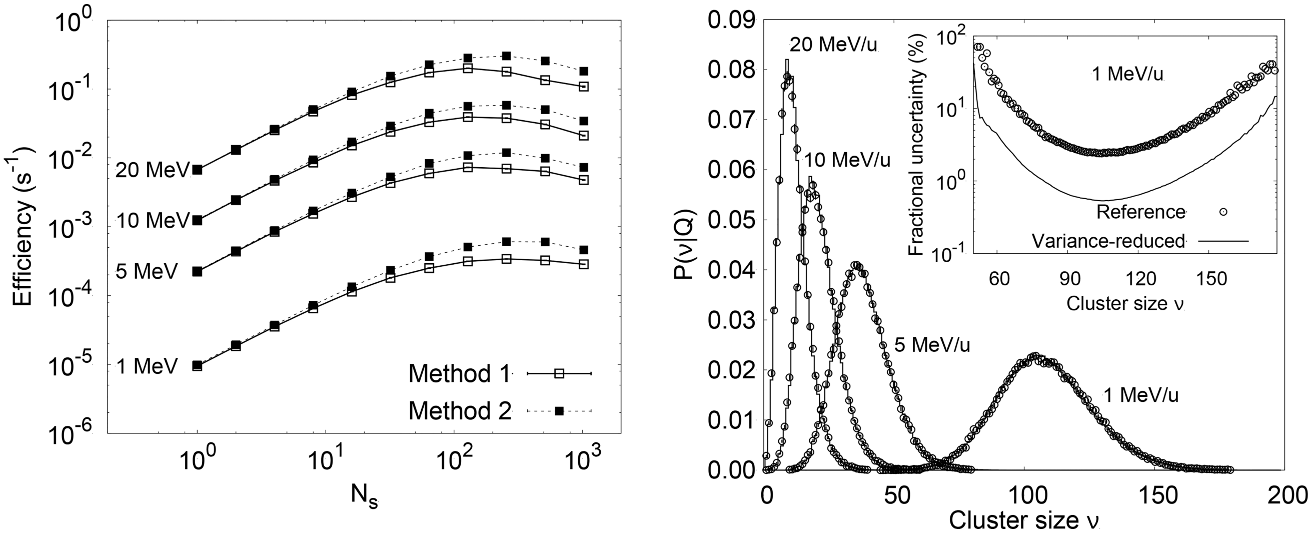

Figure 5.

Left: Relative efficiency variation with N_s for a 1, 5, 10 and 20 MeV/u carbon ion source in the cluster size simulation. The particle split was applied with the first secondary ionization. Right: Cluster size probability distributions for the same energies for the reference simulation (markers) and the variance-reduced simulations with an N_s of 128 (solid lines). The error bars on the markers represent one standard deviation. The inset shows the fractional uncertainty in percent for the probability distribution corresponding to carbon ions of 1 MeV/u.

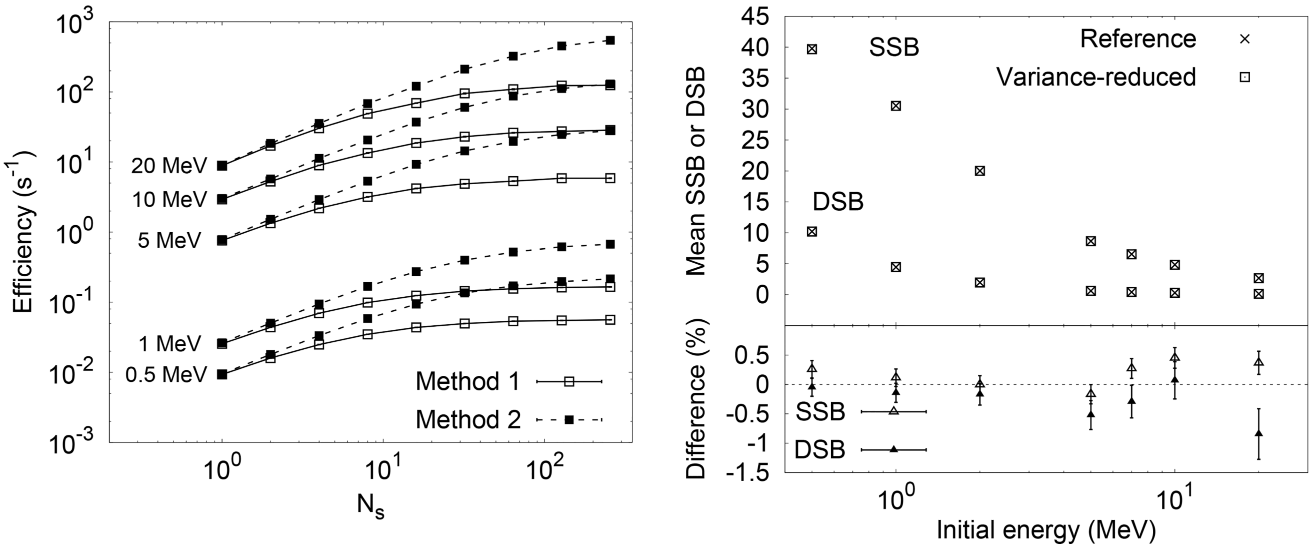

Figure 6.

Left: Efficiency variation with N_s for 0.5–20 MeV protons. Right: Mean SSB and mean DSB values for 0.5–20 MeV protons for the variance-reduced simulations with $N_s = 128$ (empty squares). The difference between the reference and variance-reduced simulation is also shown at the bottom. The error bars represent one standard deviation.

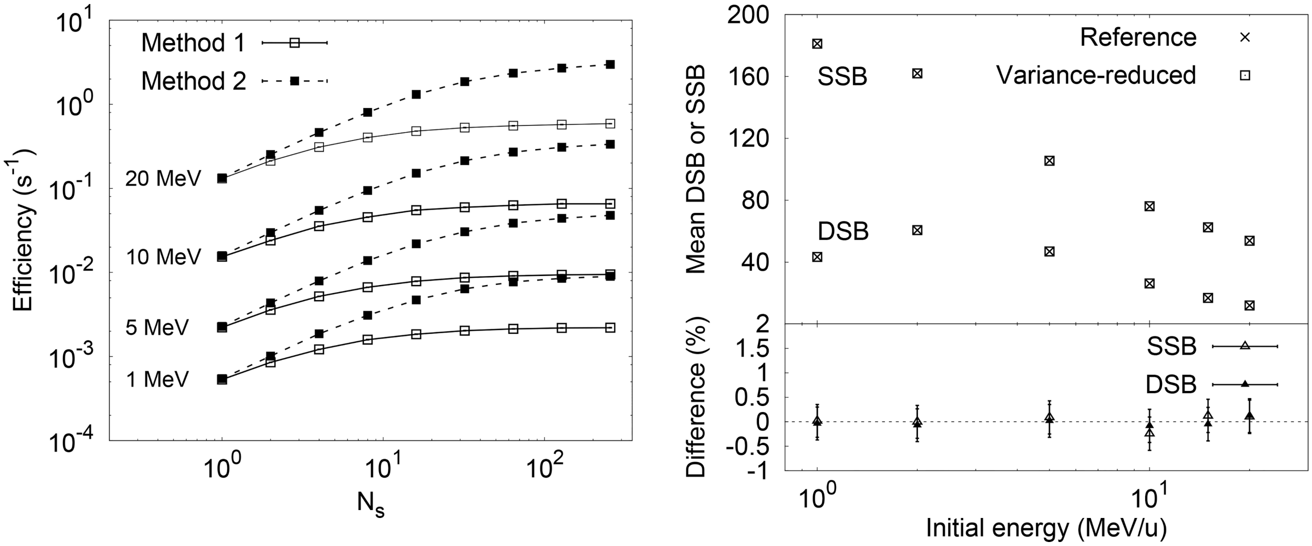

Figure 7.

Left: Efficiency variation with N_s for several energies of the incoming carbon ion source. Right: Mean SSB and mean DSB values for proton energies from 1 to 20 MeV for PST with $N_s = 128$. The relative difference in percent is also shown at the bottom. The error bars represent one standard deviation.

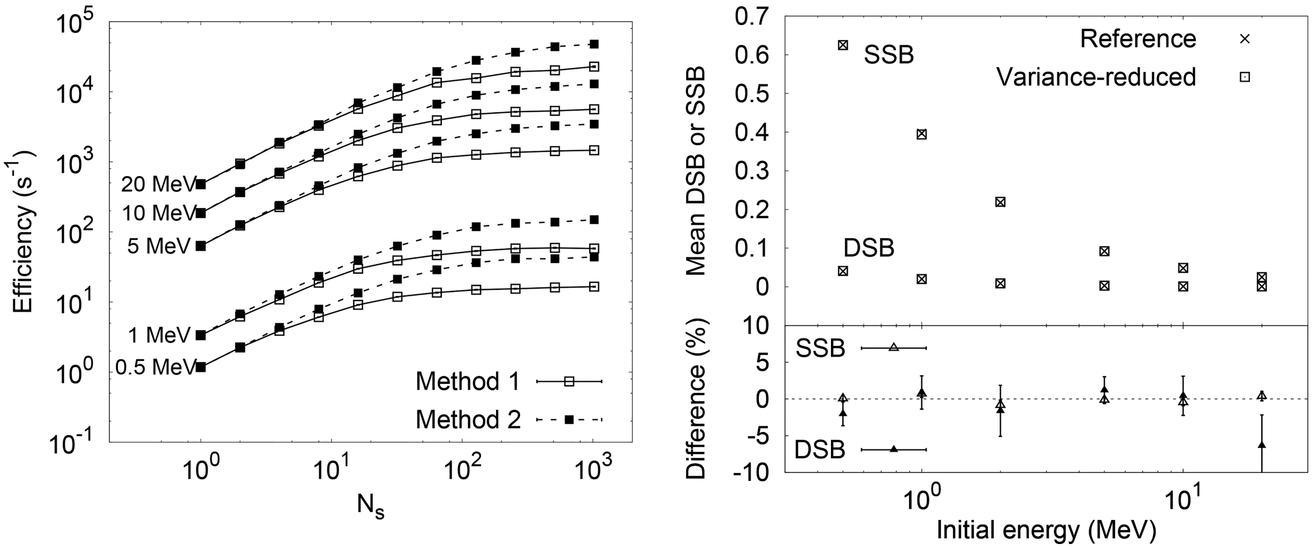

Figure 8.

Left: Efficiency variation with N_s for 0.5–20 MeV protons. Right: The mean DSB and mean SSB values as a function of energy with N_s = 128 for the variance-reduced simulations. The relative difference is also shown, with the scale on the lower left. The error bars represent one standard deviation.

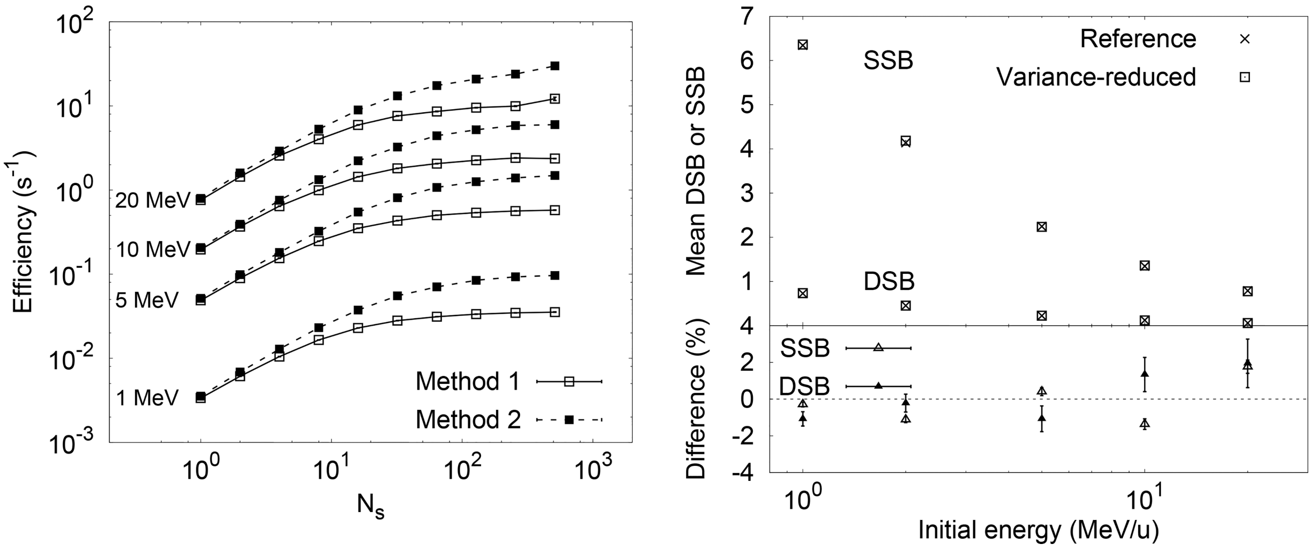

Figure 9.

Left: Efficiency variations with N_s for 1–20 MeV/u carbon ions. Right: The mean DSB and mean SSB values for 1–20 MeV/u carbon beams with $N_s = 128$ for the variance-reduced simulations. The relative difference is also shown, with the scale on the lower left axis. The error bars represent one standard deviation.

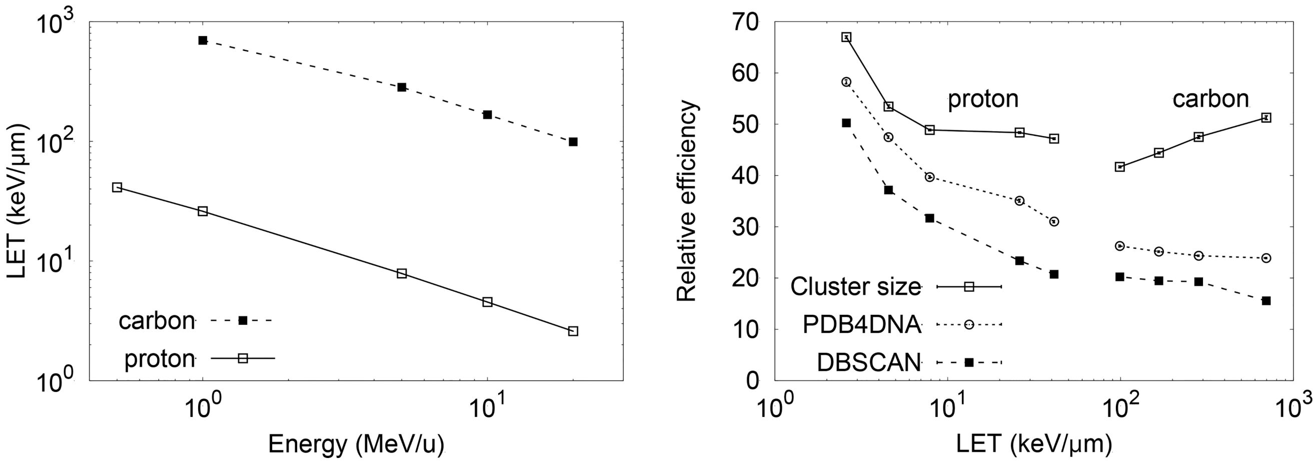

Figure 10.

Left: LET as a function of the proton and carbon ion energies simulated in this work. Right: The relative efficiency as a function of the primary particle LET for protons and carbon with $N_s = 128$. PST was implemented with Method 2.

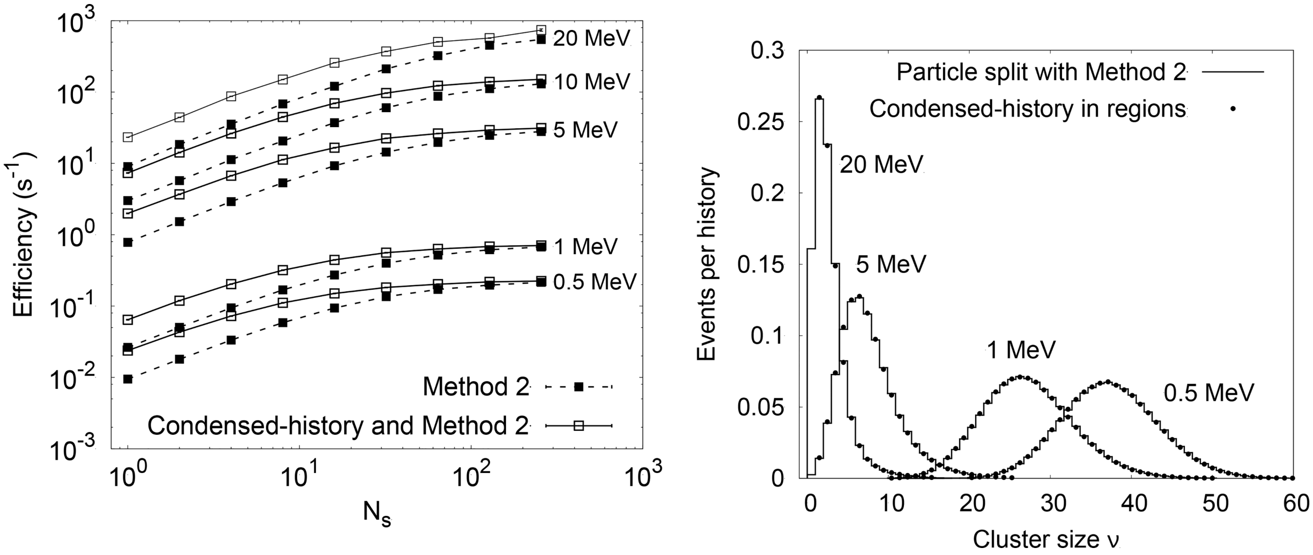

Figure 11.

Left: DBSCAN efficiency variation with N_s for proton energies from 0.5 to 20 MeV. Dashed lines with filled markers correspond to the flagged uniform PST. Solid lines with empty markers correspond to PST plus restricted transport. Right: Double strand break distributions for reference data (solid lines) and efficiency enhanced simulations (PST plus restricted transport) with N_s = 128 (points).

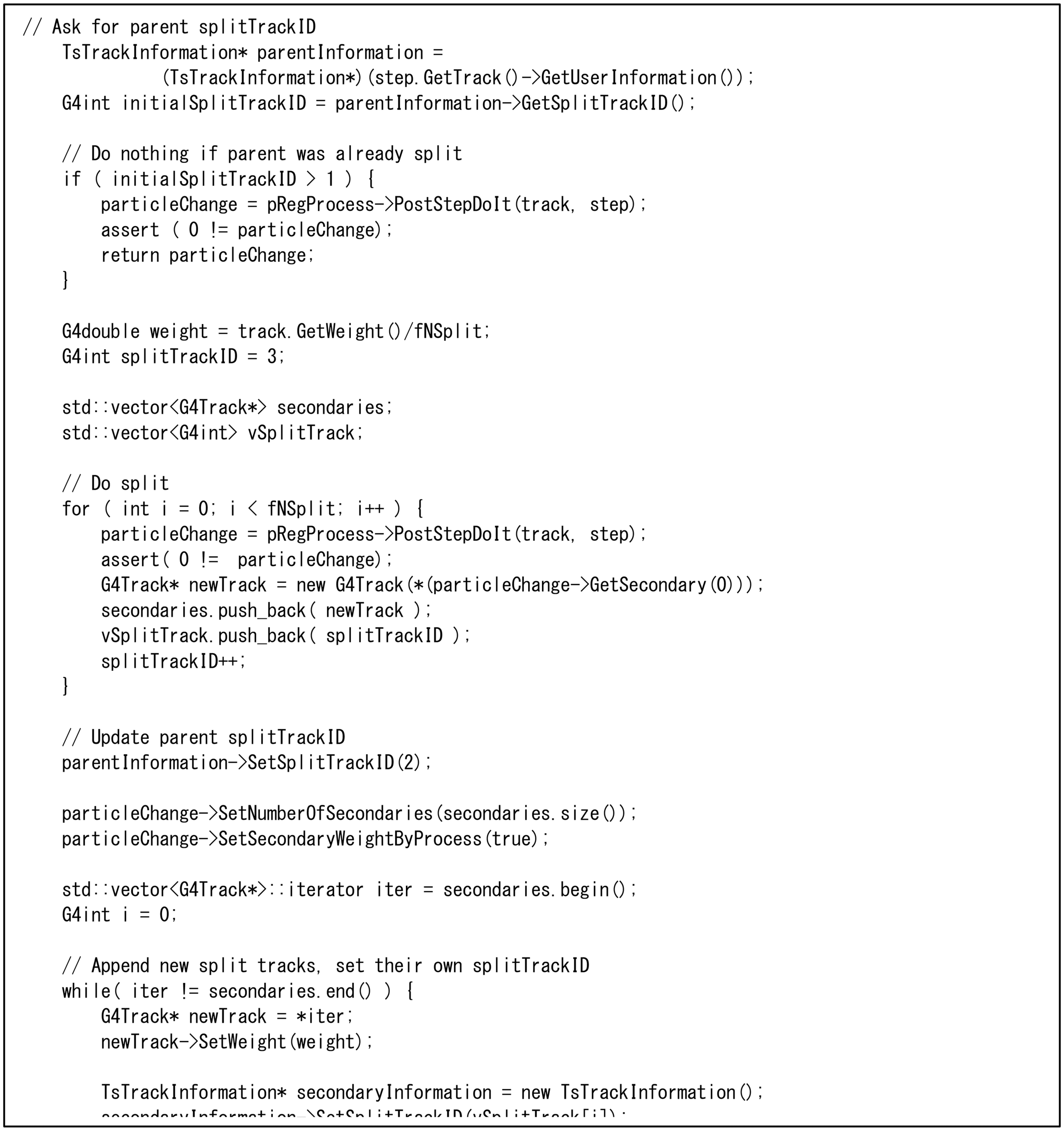

```
// Ask for parent splitTrackID
    TsTrackInformation* parentInformation =
              (TsTrackInformation*)(step.GetTrack()->GetUserInformation());
    G4int initialSplitTrackID = parentInformation->GetSplitTrackID();

    // Do nothing if parent was already split
    if ( initialSplitTrackID > 1 ) {
        particleChange = pRegProcess->PostStepDoIt(track, step);
        assert ( 0 != particleChange);
        return particleChange;
    }

    G4double weight = track.GetWeight()/fNSplit;
    G4int splitTrackID = 3;

    std::vector<G4Track*> secondaries;
    std::vector<G4int> vSplitTrack;

    // Do split
    for ( int i = 0; i < fNSplit; i++ ) {
        particleChange = pRegProcess->PostStepDoIt(track, step);
        assert( 0 !=  particleChange);
        G4Track* newTrack = new G4Track(*(particleChange->GetSecondary(0)));
        secondaries.push_back( newTrack );
        vSplitTrack.push_back( splitTrackID );
        splitTrackID++;
    }

    // Update parent splitTrackID
    parentInformation->SetSplitTrackID(2);

    particleChange->SetNumberOfSecondaries(secondaries.size());
    particleChange->SetSecondaryWeightByProcess(true);

    std::vector<G4Track*>::iterator iter = secondaries.begin();
    G4int i = 0;

    // Append new split tracks, set their own splitTrackID
    while( iter != secondaries.end() ) {
        G4Track* newTrack = *iter;
        newTrack->SetWeight(weight);

        TsTrackInformation* secondaryInformation = new TsTrackInformation();
        secondaryInformation->SetSplitTrackID(vSplitTrack[i]);
```

Code 1.

Implementation of the split process in `UserWrappedProcess.cc. GetSplitTrackID()` and `SetSplitTrackID` were previously defined in a concrete class (`TrackInformation`) derived from `G4VUserTrackInformation` as described in [34].